Title
Effective modulus of the human intervertebral disc and its effect on vertebral bone stress

Journal
Journal of Biomechanics, 49(7)

ISSN
0021-9290

Authors
Yang, Haisheng
Jekir, Michael G
Davis, Maxwell W
et al.

Publication Date
2016-05-01

DOI
10.1016/j.jbiomech.2016.02.045

Peer reviewed

HHS Public Access

Author manuscript

J Biomech. Author manuscript; available in PMC 2017 May 03.

Published in final edited form as:

J Biomech. 2016 May 3; 49(7): 1134–1140. doi:10.1016/j.jbiomech.2016.02.045.

Effective Modulus of the Human Intervertebral Disc and its Effect on Vertebral Bone Stress

Haisheng Yang[1], **Michael G. Jekir**[1], **Maxwell W. Davis**[1], and **Tony M. Keaveny**[1,2]

[1]Orthopaedic Biomechanics Laboratory, Department of Mechanical Engineering, University of California, Berkeley, CA, USA

[2]Department of Bioengineering, University of California, Berkeley, CA, USA

Abstract

The mechanism of vertebral wedge fractures remains unclear and may relate to typical variations in the mechanical behavior of the intervertebral disc. To gain insight, we tested 16 individual whole discs (between levels T8 and L5) from nine cadavers (mean ± SD: 66 ± 16 years), loaded in compression at different rates (0.05–20.0% strain/sec), to measure a homogenized "effective" linear elastic modulus of the entire disc. The measured effective modulus, and average disc height, were then input and varied parametrically in micro-CT-based finite element models (60-μm element size, up to 80 million elements each) of six T9 human vertebrae that were virtually loaded to 3° of moderate forward-flexion via a homogenized disc. Across all specimens and loading rates, the measured effective modulus of the disc ranged from 5.8 to 42.7 MPa and was significantly higher for higher rates of loading ($p < 0.002$); average disc height ranged from 2.9 to 9.3 mm. The parametric finite element analysis indicated that, as disc modulus increased and disc height decreased across these ranges, the vertebral bone stresses increased but their spatial distribution was largely unchanged: most of the highest stresses occurred in the central trabecular bone and endplates, and not anteriorly. Taken together with the literature, our findings suggest that the effective modulus of the human intervertebral disc should rarely exceed 100 MPa and that typical variations in disc effective modulus (and less so, height) minimally influence the spatial distribution but can appreciably influence the magnitude of stress within the vertebral body.

Keywords

wedge fracture; osteoporosis; intervertebral disc; finite element analysis; bone strength

Corresponding author (current address): Haisheng Yang, Department of Pediatric Surgery, McGill University, Shriners Hospitals for Children-Canada, 1003 Decarie Blvd, Montreal, H4A 0A9, Canada, yhs267@foxmail.com, yanghaisheng267@gmail.com.
Please address all reprint requests to: Tony M. Keaveny, 5124 Etcheverry Hall, University of California, Berkeley, CA 94720-1740, USA, tonykeaveny@berkeley.edu

Conflict of interest statement
The other authors do not have any conflicts of interest.

Introduction

While anterior wedge fractures are the most common type of osteoporotic spine fracture, their etiology remains unclear (Adams and Dolan, 2012; Adams and Dolan, 2011; Christiansen and Bouxsein, 2010). Presumably, an anterior wedge fracture — as opposed to a concavity fracture — occurs because the stress in the bone hard tissue is greatest in the anterior portion of the vertebral body. While cadaver experiments that apply forward-flexion loading to a vertebral body via a stiff layer of plastic do indeed produce anterior wedge-shaped fractures (Buckley et al., 2009; Dall'Ara et al., 2010; Rotter et al., 2015), experiments that load the vertebra through the disc typically produce bone failure in the trabecular bone and endplates more centrally, that is, not anteriorly (Farooq et al., 2005; Granhed et al., 1989; Hutton and Adams, 1982; Jiang et al., 2010; Landham et al., 2015). Consistent with these findings, micro-CT-based finite element analyses (Fields et al., 2010; Yang et al., 2012) have shown that, for both compression and forward-flexion loading applied via a simulated compliant homogenized disc (Young's modulus of 8 MPa), the highest stresses in the vertebral bone occur mostly centrally in the trabecular bone and endplates, whereas high stress occurs anteriorly only when the flexion loading is applied via a stiff layer of plastic (Young's modulus of 2,500 MPa).

As far as the etiology of the anterior wedge fracture is concerned, the question then arises as to what is the influence of typical variations in the disc properties on the vertebral bone stresses — can typical variations in disc properties increase the risk of an anterior wedge fracture? While the material properties and morphometry of the disc can appreciably change with aging and degeneration (Adams and Roughley, 2006; Alkalay, 2002; Inoue and Espinoza Orias, 2011; Natarajan et al., 2004), and while disc degeneration and loss of height are associated with an increased in vivo risk of vertebral fractures (Castano-Betancourt et al., 2013; Sornay-Rendu et al., 2006; Sornay-Rendu et al., 2004), it is still unclear if and how typical variations in the overall mechanical properties of a disc can influence either the location of highly stressed bone tissue within the vertebra or the overall magnitude of stress. Addressing this issue, we performed cadaver experiments to measure typical variations in a homogenized “effective” elastic modulus of the entire disc, and then varied those properties parametrically in a micro-CT-based finite element analysis of multiple vertebral bodies to determine the role of the observed typical variation in the disc properties on tissue-level bone stress in the vertebral body.

Materials and Methods

Mechanical testing of cadaveric intervertebral discs

Uniform compressive mechanical testing was performed on cadaver whole discs to measure a homogenized “effective” linear elastic modulus of the entire disc (henceforth termed the “effective modulus”). This type of measurement characterizes the average linearized behavior of the entire disc, treating it as a homogeneous elastic material. While this characterization clearly simplifies the more complex behavior of a real disc, it nonetheless provides a single metric for quantifying the mechanical behavior of the entire disc and facilitates numerical implementation of disc behavior into large-scale finite element models of whole vertebrae.

The whole-disc specimens, attached to their adjacent vertebral bodies, were prepared from 16 bone-disc-bone vertebral motion segments. These segments were disarticulated from nine anonymous donor spines aged 66 ± 16 years (mean ± SD), seven male and two female, with seven spines yielding two motion segments each and the remaining two spines yielding one motion segment each. All motion segments were between levels T8 and L5, and segments from the same spine were either neighboring or one level apart.

For each whole-disc specimen, the vertebral body portions were reinforced so that the recorded deformations of the loaded test specimens would reflect primarily the deformations of only the disc. To reinforce the specimens, the posterior elements were removed and the respective top/bottom parts (~ 5–10 mm in height) of each vertebral body were sectioned off in a transverse plane, resulting in a sectioned-vertebra/disc/sectioned-vertebra test specimen (Fig. 1A). A Dremel tool was then used to hollow out each vertebral body to within approximately 5 mm from both the endplate and the cortical shell, a water jet was used to remove any marrow, and a syringe was used to maximally fill each vertebral body with polymethylmethacrylate (PMMA). Each reinforced specimen was stored overnight at 4°C and then embedded at each end in parallel 2 mm-deep PMMA wells to provide parallel flat PMMA-surfaces for loading (Fig. 1A). Before mechanical testing, an average disc height was measured from anterior-posterior and medial-lateral radiographs. Disc degeneration was evaluated according to a five-category grading system proposed by Thompson et al. (Thompson et al., 1990).

Uniform compression testing was performed to measure the effective modulus for different strain rates. To reduce disc hydration, we applied an initial compressive load of 300 N and allowed the specimen to stress-relax for 15 minutes (McMillan et al., 1996), at which point we set the deformation reading to zero. Each specimen then underwent five dynamic preload cycles to 10% strain at a strain rate of 0.5%/s and was then compressed to failure (50% strain) at either a “low” (0.05%/s) or “high” (20%/s) strain rate. In all tests, stress was defined as the recorded force divided by the cross-sectional area of the disc and strain as the recorded platen-to-platen deformation divided by the average disc height. From the resulting stress-strain curve, we defined the effective modulus as the linearized secant modulus from the point of zero deformation to the point of maximum stress (Fig. 1B).

Parametric finite element analysis

Finite element models for six T9 vertebral bodies were adapted from those used in prior studies (Eswaran et al., 2006; Eswaran et al., 2007; Fields et al., 2010; Yang et al., 2012). In brief, six fresh-frozen T9 human whole vertebral bodies were obtained from cadavers (n = 5 male; n = 1 female; age range: 53–91 years, mean ± SD = 75 ± 15 years) with no medical history of metabolic bone disorders and then scanned with micro-CT using a 30-μm voxel size (Scanco 80; Scanco Medical AG, Brüttisellen, Switzerland). The micro-CT scans were coarsened to isotropic 60-μm voxels, segmented using a global threshold value, and the bone tissue was compartmentalized into trabecular bone, endplate and cortical shell regions. By directly converting each coarsened voxel into a finite element (Van Rietbergen et al., 1995), finite element models of each vertebral body were created, each model having up to ~ 80 million elements and over 300 million degrees of freedom. In these models, each bone

element was assigned the same linearly elastic material properties (elastic modulus of 18.5 GPa and Poisson's ratio of 0.3) and the disc was modeled as a homogeneous, isotropic, linearly elastic material that covered each endplate. Since the endplates have variable geometry, the height of the simulated disc was defined as twice the distance from the most superior or inferior end of the vertebra to an assumed line of mid-symmetry of the disc (Fig. 1C). Boundary conditions were applied to simulate 3° of moderate forward-flexion by rotating the top surface of the superior half-disc in a mid-sagittal plane about the most superior-posterior point (Fig. 1C) (Yang et al., 2012). Detailed justification of the boundary condition was explained in the Appendix.

Using these models, we conducted two parametric analyses. First, the effective modulus of the disc was varied from 8 MPa through the measured full range and a total disc height of 5 mm was assumed for these analyses. Second, using a disc effective modulus of 8 MPa, the total height of the disc was varied through the measured typical range from the experiments. In all analyses, we assumed a Poisson's ratio of 0.45 for the disc to enable appreciable disc bulging to occur upon loading (Fields et al., 2010; Yang et al., 2012).

Each (linearly elastic) finite element analysis was solved using a highly scalable, implicit finite element framework (Olympus) (Adams et al., 2004) running on a Sun Constellation cluster supercomputer (Ranger; Texas Advanced Computing Center, Austin, TX, USA). Typical hardware requirements for a single analysis comprised up to 1024 processors in parallel and 4 TB of memory. The average single-processor CPU time required for each analysis was 256 hours. Altogether, 36 analyses were performed (6 vertebrae, 3 disc modulus values, 3 disc height values), for a total single-processor CPU time of over 9,000 hours.

Finite element outcomes

To quantify the force and stress distributions within the simulated homogenized disc, we virtually divided the disc into anterior and posterior halves by a mid-frontal line passing through the geometric center and computed the ratio of the overall compressive force in the anterior half to that in the posterior half. To identify locations of vertebral bone tissue at the highest risk of failure, at the centroid of each bone element we calculated the ratio of each of the maximum and minimum principal stresses to the respective assumed tissue-level tensile (61 MPa) and compressive (150 MPa) yield strengths (Bevill et al., 2006), and defined a tissue-level risk factor as the larger ratio, which also specified the tissue-level failure mode (tensile or compressive). We then defined the high-risk tissue as the top 10% of bone tissue in the model, ranked by the tissue-level risk factor (Yang et al., 2012). The spatial distribution of the high-risk tissue within the vertebra was characterized for the entire vertebral body, and separately for the trabecular bone, endplate, and cortical shell (Fig. 1D).

Statistical analyses

For the experimental measurements, correlation analysis was used to assess any dependence on cadaver age, disc degeneration or spine level. A paired t-test was performed to assess the effect of strain rate on the measured effective modulus of the disc. For the computational outcomes, paired t-tests without Bonferroni corrections were used to determine the effect of

disc modulus and height on high-risk tissue distribution, performed separately for the trabecular bone, endplate and cortical shell regions. All statistical tests were performed using the SPSS software package (IBM SPSS Statistics, Version 22.0, IBM Corp., Armonk, NY). Statistical significance was set at $p < 0.05$. All data are presented as mean ± SD.

Results

Across all specimens and loading rates, the effective modulus of the disc varied from 5.8–42.3 MPa (Fig. 2). When tested at the low strain rate of 0.05%/s, the effective modulus was (mean ± SD) 17.0 ± 9.8 MPa and ranged from 5.8–30.9 MPa. For the higher strain rate of 20%/s, the effective modulus increased significantly to 25.5 ± 8.6 MPa ($p < 0.002$), and ranged from 17.4–42.3 MPa. As the age of the cadaver increased, the effective modulus decreased significantly for the high loading rate ($R = 0.89$, $p = 0.003$), exhibiting an approximately twofold decrease between ages 30 and 70, but did not significantly change for the low loading rate ($p = 0.059$, Fig. 2). Across all specimens, degeneration grade varied from 2–5. Effective modulus of the disc did not depend on degeneration grade in either the high ($R = 0.52$, $p = 0.18$) or low ($R = 0.57$, $p = 0.14$) strain rate groups. The average height of the disc varied from 2.9–9.3 mm and did not depend on cadaver age ($p = 0.41$, Fig. 2). The disc height increased as the spine level varied from T8 to L5 ($R = 0.77$, $p < 0.001$).

The parametric finite element analysis confirmed the expected result that the anterior half of the disc was more highly loaded than the posterior half, and this occurred regardless of varying the disc modulus or height (Fig. 3). Specifically, the axial compressive force in the disc was approximately two-fold larger in the anterior half than in the posterior half (Table 1). As the disc modulus, or height, increased from 8 to 50 MPa, or from 3 to 9 mm, the ratio of anterior-to-posterior force increased only slightly, from 2.04 ± 0.21 to 2.18 ± 0.23, or from 2.00 ± 0.22 to 2.10 ± 0.21, respectively (Table 1). However, the magnitude of the overall compressive force generated in the disc changed appreciably. As the disc modulus increased over six-fold from 8 to 50 MPa, the total compressive force in the disc increased five-fold from 2,230 ± 1,000 N to 11,230 ± 4,880 N (Table 1; $p < 0.005$ by paired t-test). A similar but smaller effect occurred as disc height was decreased, effectively making the disc behave stiffer. As the disc height was decreased three-fold from 9 to 3 mm, the total compressive force of the disc increased over two-fold from 1330 ± 520 N to 3410 ± 1670 N ($p < 0.01$ by paired t-test). When changing both the disc modulus and height, the magnitude of the stresses within the vertebra increased in the same manner as the change in overall disc compressive force.

Despite this anterior shift of disc compressive stress when disc modulus and height were varied over the observed range, most of the high-risk tissue within the vertebral body remained in the central trabecular bone and endplate (Figs. 3 and 4). Varying the disc modulus between 8– 50 MPa neither appreciably changed the distribution of high-risk tissue in the trabecular bone, endplate and cortical shell along anterior-posterior direction (Fig. 4), nor affected the distribution of high-risk tissue across all compartments of the vertebra (Fig. 5). Decreasing the disc height from 9 to 3 mm led to ~15% of the total high-risk tissue transferring from the endplate into the adjacent trabecular bone, without affecting the cortical shell (Figs. 4 and 5).

Discussion

We sought in this study to gain insight into the etiology of age-related vertebral fracture, and anterior wedge fractures in particular. Our novel experiments were designed to minimize effects of bone or endplate deformation in the measurement of what we defined as the "effective modulus" of the entire disc. Based on experimental measures of whole-disc modulus by ourselves (< 50 MPa) and others (< 25 MPa; Burns et al., 1984; Keller et al., 1987; Li et al., 1995; O'Connell et al., 2007; Pollintine et al., 2010), it seems reasonable to assume conservatively that the effective modulus of human discs, in general, does not exceed about twice the observed highest value in this experiment, namely, about 100 MPa. Our finite element analysis demonstrated that variations of this disc effective modulus across our measured typical range, and variations of disc height, did not appreciably change the spatial distribution of stress in the vertebral body — most of the high-risk bone tissue was concentrated in the central trabecular bone and endplates of the vertebra, and not anteriorly as one might expect for forward-flexion loading. However, the magnitude of the stress in the bone tissue was highly sensitive to the disc effective modulus across the measured typical range, the effect being slightly smaller for disc height. We conclude therefore, that for a moderate degree of kinematically imposed forward-flexion loading, typical stiffening or narrowing of the disc can increase stress everywhere in the vertebral body but should not redirect failure of the vertebral bone anteriorly. In this way, typical stiffening or narrowing of the disc might increase the risk of vertebral fracture generally, but not anterior fractures specifically.

The insensitivity of the spatial distribution of high-risk tissue within the vertebral body to typical variations in the effective modulus or height of the disc is somewhat surprising but insight is provided from beam-on-elastic-foundation theory (see Appendix and Fig. A1). Since high anterior stress does not develop in the vertebral bone for moderate forward flexion across the range of typical disc properties, the etiology of the common anterior wedge fracture must lie elsewhere. One possibility (Adams et al., 2006) is that anterior wedge fractures occur indirectly as a result of weak anterior bone resulting from anteriorly focused adaptive bone loss, which occurs in response to anterior stress shielding that is thought to occur as the disc loses height with degeneration and vertebral load is shifted from the vertebral body to the posterior elements during habitual activities. This theory would imply that if one were to apply forward-flexion loads on cadaver vertebrae via degenerated discs one would expect to see failure of the vertebral body in the anterior bone. However, such anterior failure has not been observed in such experiments for modest degrees of forward-flexion loading (Granhed et al., 1989; Farooq et al., 2005; Hutton and Adams, 1982; Jiang et al., 2010; Zhao et al., 2009). Those findings are consistent with our numerical results, which were derived from analysis of cadaver vertebrae that presumably underwent some form of adaptive remodeling through life.

Alternatively, it is possible that moderate forward-flexion loading is not directly associated with development of wedge fractures but that more severe forward-flexion loading is. Some experiments that used a more severe degree of forward-flexion (> ~10°) did demonstrate anterior wedge fractures, and those fractures occurred regardless of the state of disc degeneration (Adams and Hutton, 1982; Granhed et al., 1989; Luo et al., 2007). It may be

that for severe loading there is consolidation (or bottoming out) of the disc, regardless of its quality, and in that case the disc may behave much stiffer than for more normal loading. Another possible explanation, as suggested by others (Landham et al., 2015), is that modest forward-flexion loading produces initial vertebral fractures primarily in the endplates and underlying central trabecular bone — consistent with our results — and it is subsequent cyclic flexion loading, and perhaps creep (Pollintine et al., 2009), that causes progressive collapse into the anterior cortex. In that case, the observed morphology of the wedge-shaped fracture reflects merely the end result of the entire fracture process and not the initiating mechanism. In that scenario, degeneration-related disc height loss or loading at a high rate would effectively make the disc behave stiffer, leading to increased stress everywhere in the vertebral body, thus increasing the risk of fracture initiation centrally, which could eventually propagate into an anterior fracture. This result could also explain why disc space narrowing is often associated with an increased risk of vertebral fractures regardless of fracture types (Castano-Betancourt et al., 2013; Sornay-Rendu et al., 2006; Sornay-Rendu et al., 2004). Further research is required to further explore all these possible explanations.

The high sensitivity of the overall magnitude of stress within the vertebral body to the effective modulus of the disc, and less so to disc height, may have clinical implications for fracture risk assessment. Others have shown that finite element analysis derived from clinical-resolution CT scans of the spine can predict new vertebral fractures both for women and men (Wang et al., 2012; Kopperdahl et al., 2014), and can do so significantly better than can bone mineral density (BMD) as measured by dual-energy absorptiometry (DXA) (Wang et al., 2012). In those types of finite element analyses, a fixed compressive loading condition is used for all vertebrae, and a stiff layer of PMMA is placed over the endplates. If fracture risk is indeed associated with the magnitude of vertebral stress under a defined set of loading conditions, our current results suggest that further improvements to this type of clinical finite element analysis might derive from using actual patient-specific values of disc effective modulus. To date, obtaining accurate patient-specific values of disc modulus has been elusive, although our current results suggest that this may be an area of important research as far as fracture prediction is concerned.

Beyond fracture risk assessment, our results also have potential direct relevance to other applications. For example, our additional parametric studies (see Appendix and Fig. A2) indicated that high bone stresses concentrated anteriorly when the assumed effective modulus of the disc exceeded about 500 MPa. These results explain why cadaver experiments with moderate forward-flexion loading have produced anterior wedge-shaped fractures when loads are applied via a stiff layer of PMMA (Buckley et al., 2009; Dall'Ara et al., 2010; Rotter et al., 2015) but not when loads are applied via a real disc. Clinically, for patients who undergo total disc replacement or interbody spine fusion surgery, the diseased disc is often replaced by some type of stiff material or implant (Adam et al., 2003; Auerbach et al., 2010; Steffen et al., 2000). Our results suggest that those types of procedures might increase stress in the anterior bone upon moderate forward-flexion loading and in that way might increase risk of a subsequent wedge fracture in the adjacent vertebra.

The main caveat of the present study is that the entire intervertebral disc was modeled as a homogeneous isotropic elastic material when in fact it consists of the gel-like, pressurized

nucleus pulposis contained by the anisotropic multi-layered non-linearly elastic annulus fibrosus and its material properties are altered by degeneration (An et al., 2004; Iatridis et al., 1998; O'Connell et al., 2012; Wagner and Lotz, 2004; Jacobs et al., 2014). Experimentally, it is difficult to measure stress within the vertebral body, but one can measure stress in the disc, which gives some indication of the compressive axial stress acting along the endplate. For compression loading of the spine motion segment, age-related degeneration leads to a transfer of load from the nucleus to the posterior annulus (Adams et al., 2002; Adams et al., 1996). However, Forward-flexion experiments for vertebrae with both healthy and degenerated discs have shown that the disc stress does not vary substantially across the whole disc (Adams et al., 1994; Adams et al., 2000; McNally and Adams, 1992; Dolan and Adams, 2001), and that the load distribution between the anterior and posterior halves of the disc is unaffected by the degree of disc degeneration (Pollintine et al., 2004). The distinction between healthy versus degenerated disc therefore does not appear to be important for moderate forward-flexion loading, suggesting that some of the fine details of real disc behavior might not appreciably influence overall stresses acting on the vertebral endplates or within the vertebra. Indeed, our predicted distributions of disc stress and sites of initial bone failure are consistent with those from various cadaver experiments that applied such moderate forward-flexion loading via both healthy and degenerated discs (Farooq et al., 2005; Granhed et al., 1989; Hutton and Adams, 1982; Jiang et al., 2010; Landham et al., 2015). These collective findings suggest that it is reasonable to apply our results to understanding vertebral fracture for both healthy and degenerated discs despite the simplicity of how we modeled the disc. Other limitations include the small sample size for our disc specimens and our finite element models, the use of a single forward-flexion loading condition, and our use of a linearly elastic analysis to infer vertebral failure regions. Results should clearly be interpreted with these limitations in mind and are best considered in a relative sense.

In summary, our findings suggest that the effective modulus of the human intervertebral disc should rarely exceed 100 MPa and that typical variations in disc effective modulus (and less so, height) minimally influence the spatial distribution but can appreciably influence the magnitude of stress within the vertebral body.

Supplementary Material

Refer to Web version on PubMed Central for supplementary material.

Acknowledgments

Funding was provided by the National Institutes of Health (NIH AR43784). Computational resources were obtained from the National Science Foundation through the TeraGrid Program (TG-MCA00N019). TMK has a financial interest in O.N. Diagnostics and both he and the company may benefit from the results of this research.

Dr. Keaveny has served as a consultant for Amgen, AgNovos Healthcare and O.N. Diagnostics. He holds equity interests in O.N. Diagnostics.

References

Adam C, Pearcy M, McCombe P. Stress analysis of interbody fusion - finite element modelling of intervertebral implant and vertebral body. Journal of Biomechanics. 2003; 18:265–272.

Adams, MA.; Bogduk, N.; Burton, K.; Dolan, P. The Biomechanics of Back Pain. Edinburgh, Churchill Livingstone: 2002.

Adams MA, Dolan P. Vertebral fracture and intervertebral discs. Journal of Bone and Mineral Research. 2012; 27:1432. [PubMed: 22605515]

Adams MA, Dolan P. Biomechanics of vertebral compression fractures and clinical application. Archives of Orthopaedic and Trauma Surgery. 2011; 131:1703–1710. [PubMed: 21805360]

Adams MA, Hutton WC. Prolapsed intervertebral disc. A hyperflexion injury 1981 Volvo Award in Basic Science. Spine. 1982; 7:184–191. [PubMed: 7112236]

Adams MA, May S, Freeman BJ, Morrison HP, Dolan P. Effects of backward bending on lumbar intervertebral discs. Relevance to physical therapy treatments for low back pain. Spine. 2000; 25:431–437. [PubMed: 10707387]

Adams MA, McNally DS, Chinn H, Dolan P. Posture and the compressive strength of the lumbar spine. Clinical Biomechanics. 1994; 9:5–14. [PubMed: 23916072]

Adams MA, McNally DS, Dolan P. 'Stress' distributions inside intervertebral discs. The effects of age and degeneration. Journal of Bone and Joint Surgery. 1996; 78:965–972. [PubMed: 8951017]

Adams MA, Pollintine P, Tobias JH, Wakley GK, Dolan P. Intervertebral disc degeneration can predispose to anterior vertebral fractures in the thoracolumbar spine. Journal of Bone and Mineral Research. 2006; 21:1409–1416. [PubMed: 16939399]

Adams MA, Roughley PJ. What is intervertebral disc degeneration, and what causes it? Spine. 2006; 31:2151–2161. [PubMed: 16915105]

Adams, MF.; Bayraktar, HH.; Keaveny, TM.; Papadopoulos, P. Ultrascalable implicit finite element analyses in solid mechanics with over a half a billion degrees of freedom; ACM/IEEE Proceedings of SC2004: High Performance Networking and Computing; 2004.

Alkalay, R. The material and mechanical properties of the healthy and degenerated intervertebral disc. In: Barbucci, R., editor. Integrated Biomaterials Science. New York: Kluwer Academic/Plenum; 2002. p. 403-424.

An HS, Anderson PA, Haughton VM, Iatridis JC, Kang JD, Lotz JC, Natarajan RN, Oegema TR Jr, Roughley P, Setton LA, Urban JP, Videman T, Andersson GB, Weinstein JN. Introduction: disc degeneration: summary. Spine. 2004; 29:2677–2678. [PubMed: 15564916]

Auerbach JD, Ballester CM, Hammond F, Carine ET, Balderston RA, Elliott DM. The effect of implant size and device keel on vertebral compression properties in lumbar total disc replacement. The Spine Journal. 2010; 10:333–340. [PubMed: 20362251]

Bevill G, Eswaran SK, Gupta A, Papadopoulos P, Keaveny TM. Influence of bone volume fraction and architecture on computed large-deformation failure mechanisms in human trabecular bone. Bone. 2006; 39:1218–1225. [PubMed: 16904959]

Buckley JM, Kuo CC, Cheng LC, Loo K, Motherway J, Slyfield C, Deviren V, Ames C. Relative strength of thoracic vertebrae in axial compression versus flexion. The Spine Journal. 2009; 9:478–485. [PubMed: 19364678]

Burns M, Kaleps I, Kazarian L. Analysis of compressive creep behavior of the vertebral unit subjected to a uniform axial loading using exact parametric solution equations of Kelvin-solid models - Part I. Human intervertebral joints. Journal of Biomechanics. 1984; 17:113–130. [PubMed: 6725291]

Castano-Betancourt MC, Oei L, Rivadeneira F, de Schepper EI, Hofman A, Bierma-Zeinstra S, Pols HA, Uitterlinden AG, Van Meurs JB. Association of lumbar disc degeneration with osteoporotic fractures; the Rotterdam study and meta-analysis from systematic review. Bone. 2013; 57:284–289. [PubMed: 23958823]

Christiansen BA, Bouxsein ML. Biomechanics of vertebral fractures and the vertebral fracture cascade. Current Osteoporosis Reports. 2010; 8:198–204. [PubMed: 20838942]

Dall'Ara E, Schmidt R, Pahr D, Varga P, Chevalier Y, Patsch J, Kainberger F, Zysset P. A nonlinear finite element model validation study based on a novel experimental technique for inducing anterior wedge-shape fractures in human vertebral bodies in vitro. Journal of Biomechanics. 2010; 43:2374–2380. [PubMed: 20462582]

Dolan P, Adams MA. Recent advances in lumbar spinal mechanics and their significance for modelling. Clinical Biomechanics. 2001; 16(Suppl.):S8–S16. [PubMed: 11275338]

Eswaran SK, Gupta A, Adams MF, Keaveny TM. Cortical and trabecular load sharing in the human vertebral body. Journal of Bone and Mineral Research. 2006; 21:307–314. [PubMed: 16418787]

Eswaran SK, Gupta A, Keaveny TM. Locations of bone tissue at high risk of initial failure during compressive loading of the human vertebral body. Bone. 2007; 41:733–739. [PubMed: 17643362]

Farooq N, Park JC, Pollintine P, Annesley-Williams DJ, Dolan P. Can vertebroplasty restore normal load-bearing to fractured vertebrae? Spine. 2005; 30:1723–1730. [PubMed: 16094273]

Fields AJ, Lee GL, Keaveny TM. Mechanisms of initial endplate failure in the human vertebral body. Journal of Biomechanics. 2010; 43:3126–3131. [PubMed: 20817162]

Granhed H, Jonson R, Hansson T. Mineral-content and strength of lumbar vertebrae - a cadaver study. Acta Orthopaedica Scandinavica. 1989; 60:105–109. [PubMed: 2929278]

Hutton WC, Adams MA. Can the lumbar spine be crushed in heavy lifting? Spine. 1982; 7:586–590. [PubMed: 7167831]

Iatridis JC, Setton LA, Foster RJ, Rawlins BA, Weidenbaum M, Mow V. Degeneration affects the anisotropic and nonlinear behaviors of human anulus fibrosus in compression. Journal of Biomechanics. 1998; 31:535–544. [PubMed: 9755038]

Inoue N, Espinoza Orias AA. Biomechanics of intervertebral disk degeneration. Orthopedic Clinics of North America. 2011; 42:487–499. [PubMed: 21944586]

Jacobs NT, Cortes DH, Peloquin JM, Vresilovic EJ, Elliott DM. Validation and application of an intervertebral disc finite element model utilizing independently constructed tissue-level constitutive formulations that are nonlinear, anisotropic, and time-dependent. Journal of Biomechanics. 2014; 47:2540–2546. [PubMed: 24998992]

Jiang G, Luo J, Pollintine P, Dolan P, Adams MA, Eastell R. Vertebral fractures in the elderly may not always be "osteoporotic". Bone. 2010; 47:111–116. [PubMed: 20362704]

Keller TS, Spengler DM, Hansson TH. Mechanical behavior of the human lumbar spine. I. Creep analysis during static compressive loading. Journal of Orthopedic Research. 1987; 5:467–478.

Kopperdahl DL, Aspelund T, Hoffmann PF, Sigurdsson S, Siggeirsdottir K, Harris TB, Gudnason V, Keaveny TM. Assessment of incident spine and hip fractures in women and men using finite element analysis of CT scans. Journal of Bone and Mineral Research. 2014; 29:570–580. [PubMed: 23956027]

Landham PR, Gilbert SJ, Baker-Rand HL, Pollintine P, Robson Brown KA, Adams MA, Dolan P. Pathogenesis of vertebral anterior wedge deformity: a 2-stage process? Spine. 2015; 40:902–908. [PubMed: 25822544]

Li S, Patwardhan AG, Amirouche FM, Havey R, Meade KP. Limitations of the standard linear solid model of intervertebral discs subject to prolonged loading and low-frequency vibration in axial compression. Journal of Biomechanics. 1995; 28:779–790. [PubMed: 7657676]

Luo J, Skrzypiec DM, Pollintine P, Adams MA, Annesley-Williams DJ, Dolan P. Mechanical efficacy of vertebroplasty: influence of cement type, BMD, fracture severity, and disc degeneration. Bone. 2007; 40:1110–1119. [PubMed: 17229596]

McMillan DW, Garbutt G, Adams MA. Effect of sustained loading on the water content of intervertebral discs: implications for disc metabolism. Annals of the Rheumatic Diseases. 1996; 55:880–887. [PubMed: 9014581]

McNally DS, Adams MA. Internal intervertebral disc mechanics as revealed by stress profilometry. Spine. 1992; 17:66–73. [PubMed: 1536017]

Natarajan RN, Williams JR, Andersson GB. Recent advances in analytical modeling of lumbar disc degeneration. Spine. 2004; 29:2733–2741. [PubMed: 15564922]

O'Connell GD, Johannessen W, Vresilovic EJ, Elliott DM. Human internal disc strains in axial compression measured noninvasively using magnetic resonance imaging. Spine. 2007; 32:2860–2868. [PubMed: 18246009]

O'Connell GD, Sen S, Elliott DM. Human annulus fibrosus material properties from biaxial testing and constitutive modeling are altered with degeneration. Biomechanics and Modeling in Mechanobiology. 2012; 11:493–503. [PubMed: 21748426]

Pollintine P, Dolan P, Tobias JH, Adams MA. Intervertebral disc degeneration can lead to "stress-shielding" of the anterior vertebral body: a cause of osteoporotic vertebral fracture? Spine. 2004; 29:774–782. [PubMed: 15087801]

Pollintine P, Luo J, Offa-Jones B, Dolan P, Adams MA. Bone creep can cause progressive vertebral deformity. Bone. 2009; 45:466–472. [PubMed: 19465166]

Pollintine P, van Tunen MS, Luo J, Brown MD, Dolan P, Adams MA. Time-dependent compressive deformation of the ageing spine: relevance to spinal stenosis. Spine. 2010; 35:386–394. [PubMed: 20110846]

Rotter R, Schmitt L, Gierer P, Schmitz KP, Noriega D, Mittlmeier T, Meeder PJ, Martin H. Minimum cement volume required in vertebral body augmentation-a biomechanical study comparing the permanent SpineJack device and balloon kyphoplasty in traumatic fracture. Clinical Biomechanics. 2015; 30:720–725. [PubMed: 25971847]

Sornay-Rendu E, Allard C, Munoz F, Duboeuf F, Delmas PD. Disc space narrowing as a new risk factor for vertebral fracture: the OFELY study. Arthritis and Rheumatism. 2006; 54:1262–1269. [PubMed: 16572461]

Sornay-Rendu E, Munoz F, Duboeuf F, Delmas PD, Study O. Disc space narrowing is associated with an increased vertebral fracture risk in postmenopausal women: the OFELY Study. Journal of Bone and Mineral Research. 2004; 19:1994–1999. [PubMed: 15537442]

Steffen T, Tsantrizos A, Aebi M. Effect of implant design and endplate preparation on the compressive strength of interbody fusion constructs. Spine. 2000; 25:1077–1084. [PubMed: 10788851]

Thompson JP, Pearce RH, Schechter MT, Adams ME, Tsang IK, Bishop PB. Preliminary evaluation of a scheme for grading the gross morphology of the human intervertebral disc. Spine. 1990; 15:411–415. [PubMed: 2363069]

Van Rietbergen B, Weinans H, Huiskes R, Odgaard A. A new method to determine trabecular bone elastic properties and loading using micromechanical finite element models. Journal of Biomechanics. 1995; 28:69–81. [PubMed: 7852443]

Wagner DR, Lotz JC. Theoretical model and experimental results for the nonlinear elastic behavior of human annulus fibrosus. Journal of Orthopaedic Research. 2004; 22:901–909. [PubMed: 15183453]

Wang X, Sanyal A, Cawthon PM, Palermo L, Jekir M, Christensen J, Ensrud KE, Cummings SR, Orwoll E, Black DM, for Osteoporotic Fractures in Men (MrOS) Research Group. Keaveny TM. Prediction of new clinical vertebral fractures in elderly men using finite element analysis of CT scans. Journal of Bone and Mineral Research. 2012; 27:808–816. [PubMed: 22190331]

Yang H, Nawathe S, Fields AJ, Keaveny TM. Micromechanics of the human vertebral body for forward flexion. Journal of Biomechanics. 2012; 45:2142–2148. [PubMed: 22704826]

Zhao FD, Pollintine P, Hole BD, Adams MA, Dolan P. Vertebral fractures usually affect the cranial endplate because it is thinner and supported by less-dense trabecular bone. Bone. 2009; 44:372–379. [PubMed: 19049912]

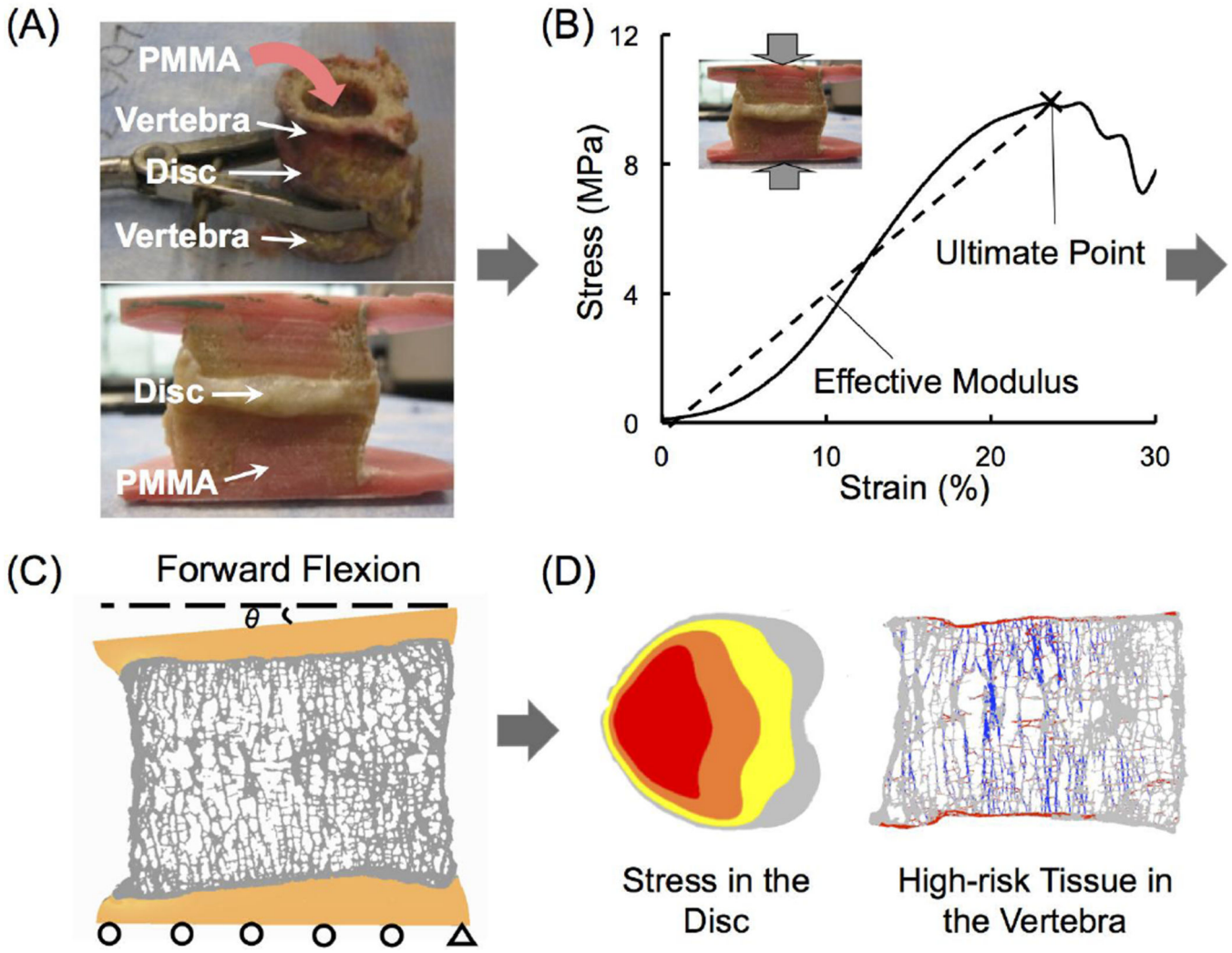

Fig. 1.

Overall study design: (A) The center of the vertebra of the bone-disc-bone motion segment was hollowed out and infilled with polymethylmethacrylate (PMMA) in order to limit any deformation of the vertebral endplates; (B) mechanical testing was performed on the bone-disc-bone preparations to measure an effective modulus of the entire disc; (C) these measurements, and those of average disc height, were used as input to a parametric finite element analysis simulating a moderate degree of forward-flexion loading ($\theta = 3°$) applied to a different cohort of vertebral specimens; (D) the main outcomes were the stress in the disc (red indicates the region being the highest loaded, gray the least) and the distribution of high-risk tissue within the vertebral body (red and blue indicate the presence of high-risk tissue in tension and compression, respectively).

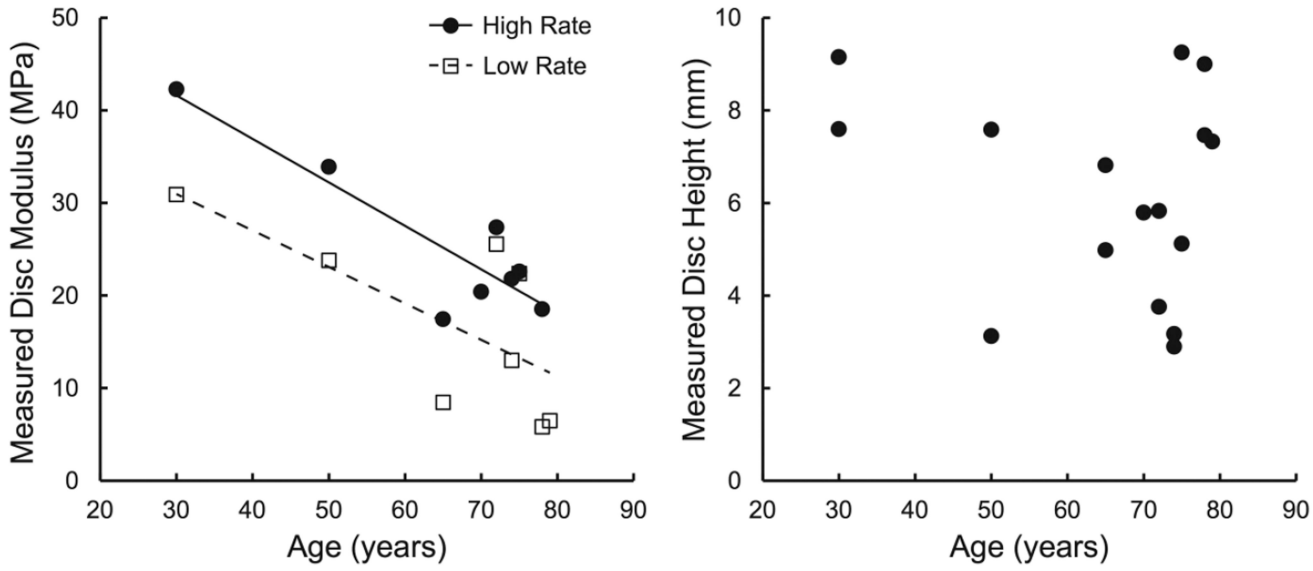

Fig. 2.

Left: Experimentally measured values of the effective modulus of the disc, versus age, for loading at a low strain rate of 0.05%/s (R = 0.67, p = 0.059) and at a higher strain rate of 20%/s (R = 0.89, p = 0.003). Right: Measured average height of the disc, versus age (R = 0.22, p = 0.41).

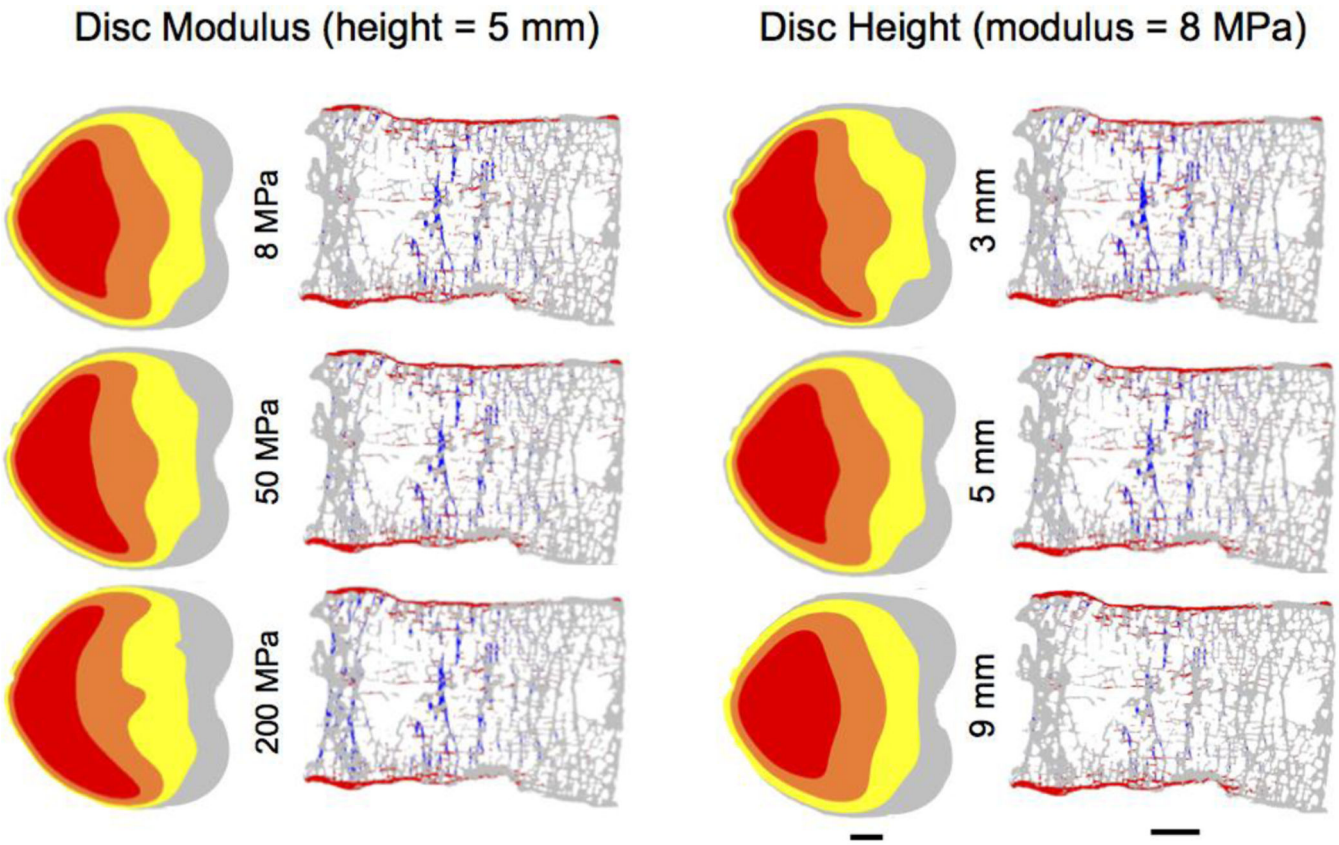

Fig. 3.

Variations in the spatial distribution of axial compressive stress at a mid-transverse section of the superior disc (colors denote quartiles, red being the highest loaded, gray the least) and the distribution of high-risk tissue at a mid-sagittal section of the vertebra (red and blue indicate the presence of high-risk tissue in tension and compression, respectively), for a typical range of values of the effective modulus and height of the disc.

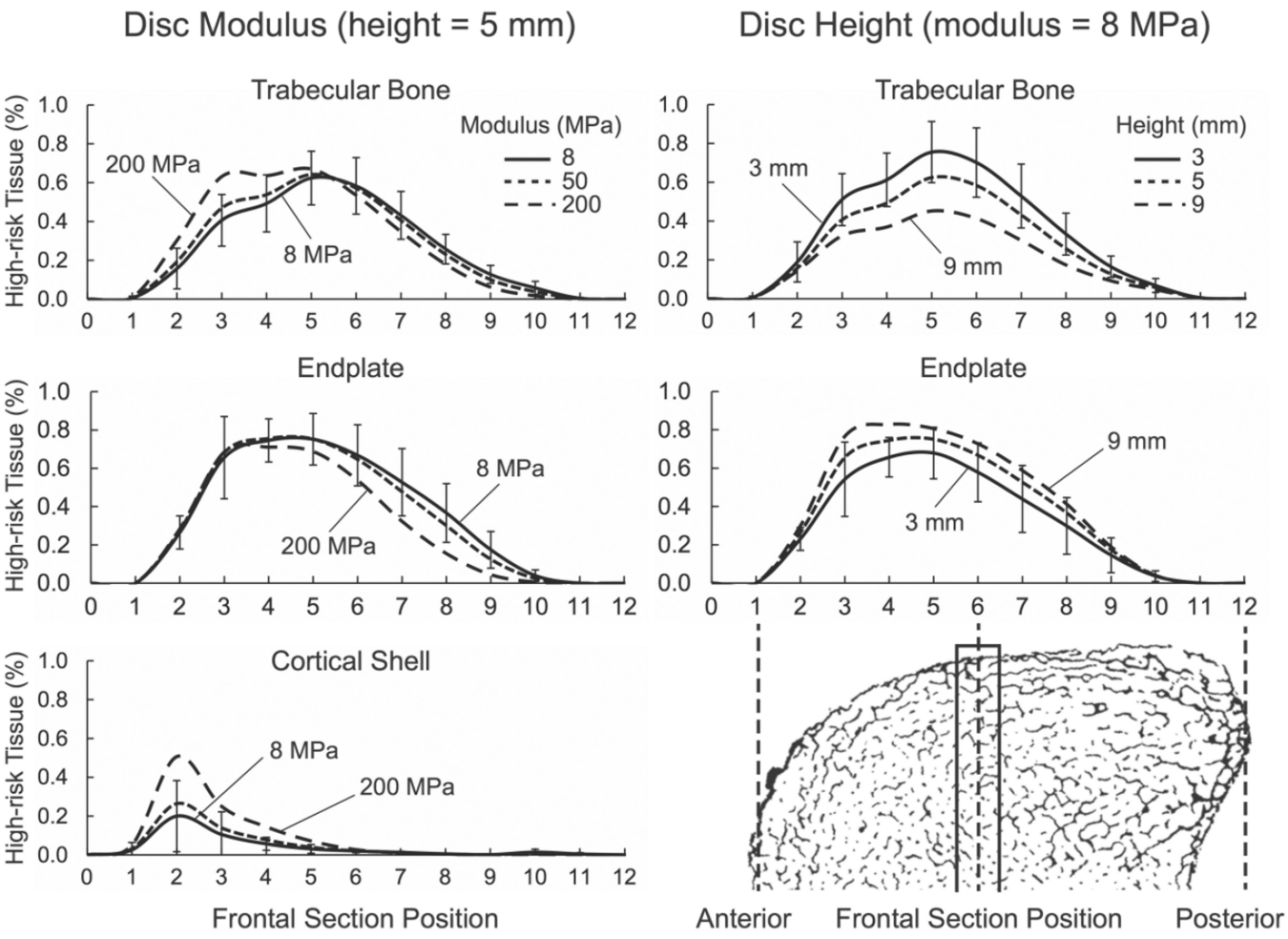

Fig. 4.

Mean variation in the amount of high-risk tissue across frontal sections of the vertebra for the trabecular bone, endplate, and cortical shell regions as the effective modulus of the disc was varied in a range of 8–200 MPa or as the height of the disc was varied from 3–9 mm (Mean response for six vertebrae; bars indicated ± 1 SD for the 8 MPa or 3 mm case). Note: one half of a transverse section of the vertebral body is only shown for illustrative purposes.

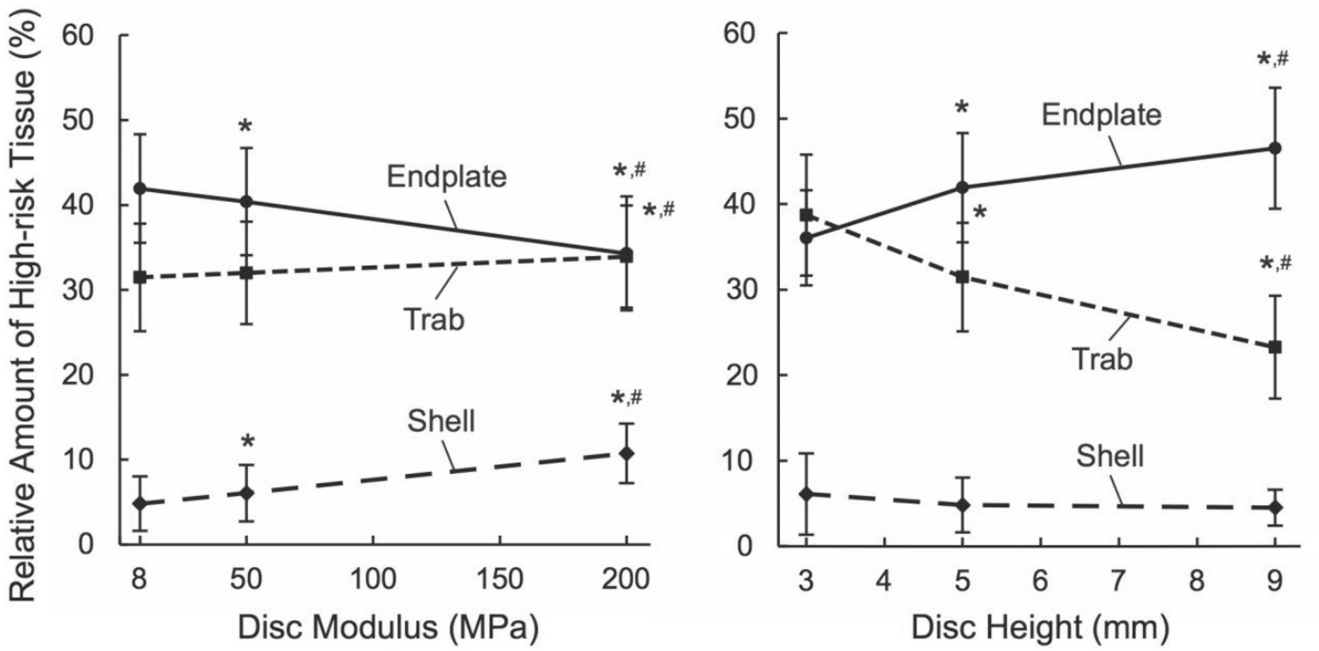

Fig. 5.

Variation in the spatial distribution of high-risk tissue in the trabecular bone, endplate, and cortical shell regions, as the effective modulus of the disc was varied in the range of 8–200 MPa (Left) or as the height of the disc was varied from 3–9 mm (Right). * The relative amount of high-risk tissue (i.e. amount of high-risk tissue in each region relative to the total amount of high-risk tissue in the entire vertebra) was significantly different from the case of the disc modulus = 8 MPa or the disc height = 3 mm ($p < 0.05$). # The relative amount of high-risk tissue was significantly different from the case of the disc modulus = 50 MPa or the disc height = 5 mm ($p < 0.01$). Bars indicate ± 1 SD.

Table 1

Net axial compressive forces acting on the anterior and posterior halves of the disc, from finite element analysis, and their ratio, as a function of the assumed effective elastic modulus and average height of the disc.

	Anterior Axial Force (N)	Posterior Axial Force (N)	Anterior/Posterior Ratio
Disc Modulus (MPa) [a]			
8	1490 ± 660	740 ± 350	2.04 ± 0.21
50	7680 ± 3280 [c]	3550 ± 1630 [c]	2.18 ± 0.23 [c]
200	19010 ± 7840 [c,d]	7790 ± 3620 [c,d]	2.48 ± 0.27 [c,d]
Disc Height (mm) [b]			
3	2270 ± 1110	1140 ± 560	2.00 ± 0.22
5	1490 ± 660 [e]	740 ± 350 [e]	2.04 ± 0.21
9	900 ± 350 [e,f]	430 ± 180 [e,f]	2.10 ± 0.21 [e,f]

Data given as mean ± SD for n = 6 T9 vertebral body specimens

[a] Disc height = 5 mm;

[b] Disc modulus = 8 MPa

[c] $p < 0.005$ compared to 8 MPa group;

[d] $p < 0.005$ compared to 50 MPa group

[e] $p < 0.05$ compared to 3 mm group;

[f] $p < 0.01$ compared to 5 mm group